Title: Underestimating global land greening: future vegetation changes and its impacts on terrestrial water loss

Authors: Yuanfang Chai [1], Chiyuan Miao[1,7,*], Louise Slater [2], Philippe Ciais[3], Wouter R. Berghuijs [4], Tiexi Chen [5], Chris Huntingford [6]

[1] State Key Laboratory of Earth Surface Processes and Resource Ecology, Faculty of Geographical Science, Beijing Normal University, Beijing 100875, China.

[2] School of Geography and the Environment, University of Oxford, Oxford OX1 3QY, United Kingdom.

[3] Laboratoire des Sciences du Climat et de l'Environnement, LSCE/IPSL, CEA-CNRS-UVSQ, Université Paris Saclay, 91191 Gif-sur-Yvette, France.

[4] Department of Earth Sciences, Vrije Universiteit Amsterdam, Amsterdam 1081 HV, Netherlands.

[5] School of Geographical Sciences, Nanjing University of Information Science and Technology, Nanjing 210044, China.

[6] Centre for Ecology and Hydrology, Wallingford, Oxfordshire OX10 8BB, United Kingdom.

[7]Lead contact

***Correspondence:** Chiyuan Miao (miaocy@bnu.edu.cn).

SUMMARY: The growing demand for water presents a significant sustainability challenge. Understanding vegetation changes is crucial, as plants significantly influence water exchange through transpiration. However, global climate models show considerable uncertainty in predicting future vegetation trends ranging from −0.007 to 0.083 $m^2\ m^{-2}\ decade^{-1}$, impacting water management. Here, we apply an emergent constraint method to reduce uncertainty in global vegetation projections for the period 2015–2100 from CMIP6, focusing on the Leaf Area Index (LAI). Our approach reduces uncertainty in global LAI projections by 37.7–53.1%. We find that this uncertainty is primarily due to incomplete representations of the CO_2 fertilization effect. Our results also show that models underestimate future LAI increases by 28.2–32.1%, leading to underestimated water loss from increased transpiration. These findings improve predictions of future vegetation and transpiration, providing valuable insights for policymakers to adjust water management strategies and better prepare for water-related challenges.

KEYWORDS: Emergent constraint; Vegetation dynamics; Transpiration; Uncertainty reduction; CO_2 fertilization effect;

INTRODUCTION

Vegetation plays a central role in regulating key Earth system processes, including carbon dynamics, water cycling, and energy exchanges between the biosphere and atmosphere[1-6]. Recent increases in global vegetation cover, often referred to as “greening”, have significant implications for terrestrial water availability. As plants absorb water from the soil and release it through transpiration, they influence regional and global water cycles. About 60–65% of terrestrial precipitation is converted

into evapotranspiration[7], with transpiration accounting for 65% of this flux[8]. Given the vital role of vegetation in these processes, the Leaf Area Index (LAI)—which measures the one-sided green leaf area per unit ground area—becomes a key parameter in understanding water and energy dynamics[9-10]. Accurate estimation of LAI is therefore critical for predicting changes in water availability and informing water management strategies in a changing climate.

Current Earth System Models (ESMs) face considerable challenges in reliably predicting future LAI changes[11]. Such uncertainty is due to simplified formulations or incorrect parameterizations of underlying biogeochemical processes and, arguably, the coarse spatial resolution of simulated LAI[12]. It has already been reported that most of the earlier CMIP5 models overestimated background global-averaged LAI [13]. Although the CMIP6 simulations have improved global area-averaged LAI time series in comparison to contemporary measurements and when compared with CMIP5 projections [3], they still display significant uncertainties. Critically, such uncertainties exist not only in model projections of mean values but also in estimated trends in LAI. The dynamics of LAI have a critical influence on vegetation growth [14-15], the terrestrial carbon cycle [16-18], and land-atmosphere feedbacks [19-21]. Therefore, the large discrepancies in global LAI projections may severely limit our understanding of future global water, carbon, and energy cycles.

The emergent constraint method is a relatively new technique to reduce the spread among ESM projections (see background and method descriptions in Note S1) and has recently gained much attention. The method exploits heuristic, and ideally physically explainable, inter-ESM empirical relationships [22-25] between some feature of current climate '*X*' and an aspect of future climate '*Y*'.

The emergent constraint approach has reduced the uncertainty of model spread in the projections of a broad range of climate attributes [26-28].

Here we introduce an emergent relationship to constrain the predicted future global LAI trends for the CMIP6 ensemble under four main future emission scenarios: SSP126, SSP245, SSP370 and SSP585 (Table S1). To verify the emergent constraint, the emergent relationship is tested out-of-sample by using models from the earlier CMIP5 ensemble (for the RCP45 and RCP85 emission scenarios, Table S2) and also using offline land surface models from the TRENDY-v9 ensemble (ensembles S1, S2 and S3, Table S3) [29], in this instance, comparing estimates for two different historical periods. Given the strong connection between LAI and transpiration, we then utilize the global LAI trends to adjust the predictions of transpiration. Our findings indicate that incorporating this emergent relationship greatly reduces uncertainty in future LAI projections, enhancing the accuracy of related transpiration estimates. These results have important implications for understanding water availability and ecosystem responses to climate change, providing valuable insights for policymakers in developing effective climate adaptation strategies.

RESULTS

Emergent constraint on future vegetation greening trend

The CMIP6 ensemble has a substantial inter-model spread in the projected long-term trend in magnitude of LAI ranging from −0.007 to 0.083 m^2 m^{-2} $decade^{-1}$ (Note S2): SSP126 (0.0068 ± 0.0083 m^2 m^{-2} $decade^{-1}$), SSP245 (0.0153 ± 0.0148 m^2 m^{-2} $decade^{-1}$), SSP370 (0.0207 ± 0.0215 m^2 m^{-2} $decade^{-1}$) and SSP585 (0.0296 ± 0.0268 m^2 m^{-2} $decade^{-1}$). To reduce the uncertainty, we fit a

linear regression to the set of points that are inter-model variations in the estimates of historical (1982–2014) and future (2015–2100) global greening trends (Figure 1A) and found a statistically significant empirical relationship between them (Figure 1A). This relationship, which provides an emergent constraint (See Methods), holds under all four emission scenarios of SSP126, SSP245, SSP370 and SSP585 (Figure 1A and Figure S3, $0.85 \leq r \leq 0.96$ across the four SSPs, p value<0.001). This type of emergent constraint (i.e., based on projecting a variable onto itself) is particularly robust, as it relies on the same physical mechanisms for both the predictor and the predictand, leading to a very high correlation coefficient for the emergent relationships (Note S3). Given this statistically significant relationship across the CMIP6 models, we can impose a constraint on future global greening by using the CMIP6-based relationship and an observational estimate of global greening trends for the recent historical period (from three observational datasets: Global Mapping LAI (GLOBMAP v3) [30], Global Land Surface Satellite LAI (GLASS) [31] and Global Inventory Modeling and Mapping Studies LAI4g (GIMMS LAI4g) [32]). The hierarchical emergent constraint procedure proposed by Bowman et al.[33], which provides a robust approach for constraining future Earth system projections (See Method), is applied to narrow the inter-model spread in expected future LAI trends. This method enables us to account for the observational uncertainty across the three LAI datasets.

After applying the constraint, we found that the raw CMIP6 ensemble mean underestimates the expected future global greening trends by 32.1%, 29.8%, 30.9% and 28.2% for the emission scenarios SSP126 to SSP585, respectively (Figure 1B and Figure S3). Hence, we estimate that the future global mean LAI trends are likely to reach higher values of 0.010 ± 0.005 m^2 m^{-2} $decade^{-1}$ (SSP126, mean ± one standard deviation), 0.022 ± 0.007 m^2 m^{-2} $decade^{-1}$ (SSP245), 0.030 ± 0.010 m^2

111 m^{-2} $decade^{-1}$ (SSP370) and 0.041 ± 0.013 m^2 m^{-2} $decade^{-1}$ (SSP585). In addition to constraining mean
112 trends, these values also indicate that the emergent constraint narrows the span of the PDFs of the
113 constrained LAI. Such refinement lowers the uncertainty ranges of the future global greening trends
114 by 37.7–53.1% (Figure 1B and Figure S3). The aforementioned emergent constraints are minimally
115 affected by land cover changes (LCCs, Note S4).
116
117 Winkler et al.[34] demonstrated that analysing different future time periods or different durations may
118 affect any emergent relationship. To assess emergent relationship sensitivity and to test the effects of
119 future time period length, we rebuilt emergent relationships between the historical LAI trend during
120 1982–2014 and the future LAI trend during periods of different duration. Specifically, we considered
121 future periods ranging from 30 years (2015–2044) to 86 years (2015–2100). We found that the
122 constrained LAI trends consistently reveal an underestimation of future global greening trends by the
123 CMIP6 models, irrespective of the duration of the future period considered (Figure S6). The
124 emergent relationships are significant for each time period length ($r \geq 0.89$, Figure S7). In addition,
125 we employed a 30-year moving window analysis. Under the emission scenarios of SSP245, SSP370,
126 and SSP585, the correlation coefficients of the emergent relationships remain significant across
127 different moving time windows (p value < 0.01, Figure S8). The CMIP6 models consistently
128 underestimated the future global mean LAI trend across all moving time windows, and the
129 application of the emergent constraints substantially reduced uncertainty in each case. In contrast,
130 under the SSP126 scenario, the correlation coefficients of the emergent relationships became
131 non-significant after 2050 (Figure S8). This change occurs because, under the sustainable "green"
132 pathway of SSP126, atmospheric CO_2 trends peak after 2050 and subsequently decline. CO_2 acts as a

key driver for LAI growth, and the shift in CO_2 dynamics after 2050 greatly alters this fertilization effect, disrupting the physical mechanisms behind the emergent relationships. Comparing the results over the full period of 2015–2100 with those from the shorter period of 2015–2050, we were pleased to find that there is an improvement in the emergent relationships when using the shorter period of 2015–2050, with correlation coefficients increasing from 0.85 to 0.95 (Figure S9). Applying the emergent constraint once again confirms that future LAI trends are indeed underestimated by the CMIP6 models.

Confirming the robustness of the emergent constraints

Hall et al.[35] and Williamson et al.[36] suggest using out-of-sample testing to assess the robustness of mechanisms underpinning an emergent constraint. We thus tested the same emergent constraint but now for the earlier CMIP5 model ensemble. For the CMIP5-based calculations, we again found a significant emergent relationship between the historical (1982–2005) and the future (2015–2100 under RCP45 and RCP85) global LAI trends (Figure 1C and Figure S10, $0.69 \leq r \leq 0.83$, p value<0.001). Importantly, as in the case of the CMIP6 models, these emergent constraints illustrate that the CMIP5 models also underestimated the future increasing rates of global LAI (by 14.8–17.2%, depending on the RCPs, Figure 1D and Figure S10). The uncertainties of the future LAI trends are also reduced by 14.4–21.6% in comparison with the original CMIP5 predictions. The constrained results, therefore, remain broadly invariant between the CMIP5 (Figure 1D) and CMIP6 (Figure 1B) ensembles, providing further support for the robustness of these results.

Most CMIP6 models have been developed based, to some extent, on their previous version in the

CMIP5 ensemble, suggesting the two generations of ESMs are not entirely independent. Thus, we further tested the emergent constraints by using an arguably more independent model ensemble, TRENDY-v9. Such independence is due to this ensemble consisting of 15 terrestrial carbon cycle models, two thirds of which are not used as the land component of CMIP6 ESMs. We found a nearly linear emergent relationship between the "*historical*" (1982–2000) and the "*pseudo future*" (2001–2019) global greening trends across the TRENDY-v9 models under all three numerical experiments ($0.97 \leq r \leq 0.98$, Figure S11 and Note S5), again supporting the robustness of the emergent constraints. After constraining by using observations during 1982–2000, the newly estimated global greening trends under all three controlled experiments are much closer to the real rate of increase from the observations during 2001–2019 (Figure S11), with the discrepancy between the simulations and the observations reduced by 32.8–77.2%.

Applications of emergent constraints at regional scale

We explored our LAI-based emergent constraints for six continents and three main tropical regions, henceforth referred to as the American rainforest, African rainforest and Asian-Australian rainforest. Statistically significant emergent relationships between the past and the future greening trends under the four emission scenarios from SSP126 to SSP585 were successfully established for all nine sub-regions ($0.55 \leq r \leq 0.98$ across the nine sub-regions under four SSPs, p value<0.05, Figure 2 and Figures S17–19). When combined with observational data, the constrained results indicate that the raw CMIP6 predictions underestimate future land greening trends across all six continents and in the three rainforest regions (Figure 2 and Figures S17–19). This highlights the need for more accurate assessments of regional greening trends. This finding underscores the importance of refining climate

177 projections to better inform regional ecosystem management and adaptation strategies. The new
178 regional constrained estimates of future LAI trends for the SSP585 scenario are 0.036 ± 0.021 m^2 m^{-2}
179 $decade^{-1}$ (mean ± one standard deviation) for North America, 0.042 ± 0.021 m^2 m^{-2} $decade^{-1}$ for
180 Europe, 0.041 ± 0.013 m^2 m^{-2} $decade^{-1}$ for Asia, 0.032 ± 0.025 m^2 m^{-2} $decade^{-1}$ for Africa, 0.031 ±
181 0.020 m^2 m^{-2} $decade^{-1}$ for South America, 0.022 ± 0.017 m^2 m^{-2} $decade^{-1}$ for Australia, 0.035 ± 0.028
182 m^2 m^{-2} $decade^{-1}$ for the American rainforest, 0.063 ± 0.047 m^2 m^{-2} $decade^{-1}$ for the African rainforest
183 and 0.057 ± 0.030 m^2 m^{-2} $decade^{-1}$ for the Asian-Australian rainforest (Table S4). As with the global
184 calculations, for all regional locations these emergent relationships also markedly reduce the
185 inter-model spread in greening trends by 7.4–65.8% (i.e., lower standard deviations), depending on
186 the SSPs and sub-regions.
187
188 **Hydrological implications of global greening trends**
189 The relationship between LAI and transpiration is closely intertwined. A higher LAI typically
190 indicates that plants can capture more light energy, enhancing photosynthetic efficiency, promoting
191 growth, and increasing transpiration capacity [37-39]. As LAI increases, there is often a corresponding
192 rise in the number of stomata and stomatal conductance, facilitating the evaporation of water from
193 the leaf interior into the atmosphere [40-41]. Additionally, a higher LAI demands more water from plants,
194 which can lead to water stress during drought conditions, impacting their physiological functions [42].
195 Furthermore, LAI influences the surrounding microclimate by enhancing shading effects, which can
196 lower soil temperatures and transpiration rates [43-45]. Consequently, uncertainties in LAI can
197 propagate to uncertainties in transpiration by affecting stomatal conductance, water demand,
198 photosynthetic efficiency, microclimate conditions, and ecosystem responses [46]. The interactions

among these factors may result in notable discrepancies in transpiration projections across different ESMs. Hence, we sought to determine the implications of the underestimated global greening trends for future global transpiration. If there is sufficient water availability in soils to meet the evaporative demand of vegetation, transpiration can be expected to be controlled by the extent of vegetation leaf area, thereby depending directly on LAI. We find substantial evidence of this suggestion when studying the relationships between the historical global mean LAI trend and the future global mean transpiration trend, as projected by CMIP6 models. However, this finding, as derived at the global scale across the CMIP6 models, is only valid under the low and middle emission scenarios of SSP126 (r=0.77, p value<0.01, Figure 3A) and SSP245 (r=0.76, p value<0.01, Figure 3B) [47].

The significant emergent relationships under the SSP126 and SSP245 scenarios (Figure 3) explain more than half of the variance of the global mean transpiration trends projections across the CMIP6 models. The remaining variance might be explained by stomatal behavior, canopy light use, interception loss, and root water uptake processes that are not considered in the regression. By combining the regression relationship with the observations, we estimate that the future trend of global monthly transpiration increase during 2015–2100 is 0.0138 ± 0.0077 mm month^{-1} year^{-1} (SSP126, Figure 3A) or 0.0136 ± 0.0099 mm month^{-1} year^{-1} (SSP245, Figure 3B). Similar to LAI trends, these trends in transpiration are higher than when considering the ESM simulations without applying any constraint. Specifically, we estimate that future transpiration increases have been underestimated by 24.6% and 31.1%, respectively, relative to the original CMIP6 predictions of 0.0104 ± 0.0111 mm month^{-1} year^{-1} (SSP126) and 0.0094 ± 0.0141 mm month^{-1} year^{-1} (SSP245). This underestimation suggests that future increases in terrestrial water availability may be

overestimated by 29.9% to 48.2%, highlighting the urgent need for a comprehensive assessment of future climate change impacts on water resource management to prevent unsustainable water use. Furthermore, the significant underestimation of the transpiration processes by the ESMs also implies largely underestimated values of the future transpiration to evapotranspiration ratio, which have also been identified in the CMIP5 models for the period of 1980–2005 by Lian et al.[46]. Besides constraining the mean future transpiration trend, the emergent constraint approach also lowers the standard deviations by 29.6–30.8% (Figure S20) compared to the original CMIP6 outputs. The substantially higher future rates of LAI-driven transpiration may indicate a raised risk of water shortage in the future, due to related lower soil moisture content.

DISCUSSION

Verifying mechanisms underpinning emergent constraints

Accurate prediction of LAI is essential for understanding transpiration processes, which are a vital component of the water cycle. Transpiration affects the availability of regional water resources by transferring water moisture from the soil to the atmosphere. An elevated LAI can lead to excessive extraction of soil moisture by plants to meet their transpiration needs, potentially threatening the sustainability of regional water resources. Therefore, improving the accuracy of LAI predictions is crucial, as it allows for more precise assessment and management of water resources, facilitating effective utilization in agriculture, forestry, and urban planning. However, existing ESMs exhibit significant uncertainty in forecasting changes in LAI. A major challenge stems from the unclear mechanisms contributing to the uncertainties in future LAI trends predicted by the models, resulting in a substantial knowledge gap. Understanding the mechanistic links that explain the emergent

243 relationship between model diagnostics predicting historical quantity X and their future estimates of
244 quantity Y helps identify the underlying causes of uncertainty in LAI predictions. [35]. Here we start by
245 individually regressing the global mean LAI trend against the trend in (or the mean value of) global
246 water availability, nitrogen in soils, air temperature and length of the growing season across the
247 CMIP6 models. However, we find relatively weak linear correlations between these variables across
248 models and under all SSPs, for both past and future periods ($-0.4 \leq r \leq 0.50$, *p value*>0.01, Figure S21).
249 This suggests that these driving factors have relatively little influence on the LAI trend spread at the
250 global scale.
251
252 Increasing atmospheric CO_2 concentration enhances plant photosynthetic carbon fixation rates (this
253 is the CFE) [48], and this has been found to explain approximately 70% of the observed global greening
254 phenomenon, followed by nitrogen deposition (9%), climate change (8%) and land cover change
255 (4%) [49-50]. Thus, it can be assumed that models with different CFE may predict different future LAI
256 trends. To test this assumption, we estimated the sensitivity of LAI to climate variations by
257 performing a multi-linear regression of annual mean LAI anomalies with CO_2, air temperature and
258 precipitation (Note S6). We used the regression coefficients to estimate the effects of the physically
259 relevant driving factors on vegetation dynamics, which is an approach similar to previous studies [51-52]
260 (Note S6). We found that the sensitivity of LAI to CO_2 has a nearly linear relationship with global
261 mean LAI trends across the CMIP6 models during both the past (1982–2014, r=0.88, Figure S21)
262 and future periods (2015–2100, $0.82 \leq r \leq 0.91$ under the four SSPs). This indicates the dominant role
263 of CFE in driving the large inter-model spread in LAI trends across ESMs. As an additional test, we
264 also investigated model projections from the Coupled Climate Carbon Cycle Model Intercomparison

Project (C4MIP) (Figure S22). The C4MIP runs provide separate radiatively and biogeochemically coupled experiments, which enable us to separate and quantify the sensitivity of vegetation dynamics to changes in atmospheric CO_2 concentration [53]. We found a series of significant relationships between future CFE and future global mean LAI trends across the C4MIP models (r=0.84, Figure S22). This indicates that the models with high CFE tend to predict a high future global mean LAI trend, while the models with low CFE tend to have a low global mean LAI trend. Therefore, our findings support the key role of CFE in driving LAI uncertainties, with a contributing of 71%.

Drivers of uncertainty in transpiration projections

In contrast to the strong correlations shown in Figure 3 under low emission scenarios, the correlations of the emergent relationships between historical global mean LAI trends and future global mean transpiration trends are weak for the higher emission scenarios of SSP370 and SSP585 ($r \leq 0.28$, Figure S23). A possible reason for these last two relationships being statistically insignificant is that, although the vegetation leaf area is enhanced under the high emission scenarios of SSP370 (0.030 $m^2\ m^{-2}\ decade^{-1}$) and SSP585 (0.041 $m^2\ m^{-2}\ decade^{-1}$), compared to SSP126 (0.010 $m^2\ m^{-2}\ decade^{-1}$) and SSP245 (0.022 $m^2\ m^{-2}\ decade^{-1}$), the spatial extent of terrestrial drying (reduced soil water content) is also enhanced by 30.2%. These high future soil water limitations occur over more than half of the Earth's land surface under the SSP370 and SSP585 scenarios [54]. Therefore, although high increases in LAI are projected under SSP370 and SSP585, the lower soil water availability offsets this increase and becomes a limitation to future transpiration. As such, LAI changes may therefore contribute less to the inter-model spread of future transpiration changes under the high emission scenarios (Figure S23). The uncertainty sensitivity analysis further demonstrates

that uncertainty in future LAI trends significantly contributes to uncertainty in future transpiration trends under the low and middle emission scenarios (Note S7). Conversely, under the high-emission scenarios (SSP370 and SSP585), as soil moisture declines, its influence on transpiration becomes more pronounced, with uncertainties in future surface soil moisture trends exerting a greater impact on future transpiration uncertainties (Note S7).

Implications of underestimated vegetation on warming

In addition to transpiration, the overall land surface water and energy balance is also highly sensitive to predicted LAI trends[7,55-56]. Recent studies have indicated that the global greening phenomenon has slowed down the increase of the global mean land surface air temperature by 0.09 ± 0.02 °C since 1982 (i.e., 12% of global warming) [57]. This slowdown is due to the cooling effects from the increased evapotranspiration [56]. Therefore, our discovered underestimate of future global vegetation suggests that greening may play a stronger role in cooling the land surface air temperature than hitherto expected. As a consequence, our work implies that future global warming trends might be overestimated by the ESMs when aggregated globally. Indeed, a recent study indicates that the CMIP6 models overestimate the future global mean air temperature increases in 2090 by 14–16%, relative to 1995–2014 [22], and we offer the possibility that this may be partially due to inaccuracies in simulating LAI. A counterargument to this is that stomata closure in response to higher CO_2 levels could limit transpiration and thus may offset some of the cooling due to higher LAI values [58]. This closure effect might be especially strong in temperate, boreal and tropical forests but less evident in grasslands (see discussion in Note S8).

In summary, our constraint provides a powerful benchmark to those responsible for enhancing process representation in the land part of ESMs and in particular including components that influence simulated LAI response to rising CO_2 levels. Such improvements may enable better simulations of carbon allocation between different land carbon pools as the climate changes, as well as improved depiction of terrestrial geochemical cycles that interact with the full global carbon cycle. Our second constraint reveals that the underestimation of the greening trends implies that there may also be an underestimation by the ESMs of increases in future water losses from the land to the atmosphere. Higher water losses may exacerbate any future shortages of water resources. Lastly, we noted that the predictive capability by any emergent constraint may diminish if key certain processes are not accounted for in any ESM. This concern becomes particularly significant if such processes become more important as climate change increases. One example is that very few land components of ESMs describe drought impacts on vegetation mortality, which may become more important as global warming increases. It is noteworthy that the emergent constraint method has inherent limitations. While this approach seeks to enhance estimates of future Earth system dynamics, several factors can influence the reliability of emergent constraint (Note S5). Observational uncertainties, incomplete integration of land cover changes into ESMs, and significant fluctuations in global land surface temperatures may impact the accuracy of the constrained results. Additionally, reliance on single historical variables and the use of linear relationships may not adequately capture the complexities of nonlinear interactions among multiple climate variables. Acknowledging these limitations can refine the applicability and effectiveness of the emergent constraint approach.

Methods

Selection of models and observational data sets

To build emergent relationships, we collected monthly LAI data from 18 models of the Coupled Model Intercomparison Project Phase 6 (CMIP6) during the historical period (1982–2014) and the future period (2015–2100) under the four Shared Socio-economic Pathways scenarios (SSP126, SSP245, SSP370 and SSP585, and where additional to scenarios of future atmospheric concentrations of greenhouse gas, they also provide pathways in atmospheric aerosols and notably land-use changes). The Norwegian Earth System Models (NorESM2-LM and NorESM2-MM) and the Community Earth System Models (CESM2 and CESM2-WACCM) are excluded from these 18 models because they predict unrealistic future tropical LAI increases [59] (Note S9). These models share much of the same code and components, resulting in nearly identical land dynamics (Note S9). To assess the robustness of our proposed emergent constraints, we also collected for analysis historical and future outputs from 17 CMIP5 models under the emission scenarios of RCP45 and RCP85. The monthly data from 15 terrestrial carbon cycle models of TRENDY-v9 during the period 1982–2019 was also used to test the emergent relationships. After identifying a series of emergent relationships between past and future global mean LAI trends, we used the observed estimates of global LAI trends from the remote sensing datasets to obtain the constrained future LAI trends (GLOBMAP, GLASS and GIMMS LAI4g). Based on extensive validations for all biome types against field measurements and other satellite products, it has been demonstrated that these datasets provide a reliable estimate of global LAI trends with high quality and accuracy[32,60-61].

Hierarchical emergent constraint framework

Traditional emergent constraints proposed by Cox et al.[27] provide a quantitative, probabilistic

framework for estimating equilibrium climate sensitivity based on observations and the current climate. However, their formulation lacks an explicit consideration of observational uncertainty [27]. The hierarchical emergent constraint framework provides a robust approach for constraining future projections of Earth system features because it considers the correlation between present and future Earth system features, the bias between observations and the model ensemble mean, and the observation uncertainty [33]. This method inherently possesses recursive characteristics through the use of conditional distributions, which encompass data assimilation techniques, such as Kalman filtering [33]. These techniques are utilized in various forms within numerical weather prediction [62]. Additionally, this approach has been applied in the realm of climate analysis, covering areas like regional climate forecasting and the detection and attribution of climate change [63-64]. The method requires data for a projected future Earth system variable (y), a simulated historical Earth system variable (x) and an observed current Earth system variable (x_o) [33]. Least-squares linear regression is applied to develop the emergent constraint relationship between x and y (equation (1)) [23]:

$$y = a(x - \bar{x}) + \bar{y} \tag{1}$$

where a is the regression coefficient, which can be calculated by using equation (2); $\bar{y}$ and $\bar{x}$ are the multi-model ensemble mean values of y and x, respectively.

$$a = \rho \frac{\sigma_y}{\sigma_x} \tag{2}$$

Here, ρ is the correlation coefficient between y and x; σ_y and σ_x are the standard deviations of y and x, respectively, across an ESM ensemble. The observed current Earth system variable x_o is used to constrain y, and thus we need to consider the uncertainty in the observations. Assuming that the observation is related to the current Earth system variable through the additive-noise model under

375 Gaussian assumptions, we use the signal–noise ratio (SNR) in the observed current Earth system
376 variable to correct the scaling factor *a* (equation (3)) [33,65].

377 $$a^* = \frac{1}{1+SNR^{-1}}a \quad (3)$$

378 The SNR defines the relative strength of the signal variability to the noise variability [33], estimated by
379 using equation (4), where σ_x^2 and σ_o^2 are the variances across the models and across the different
380 observational datasets, respectively.

381 $$SNR = \frac{\sigma_x^2}{\sigma_o^2} \quad (4)$$

382 If the noise dominates the signal, the forecast anomaly will be close to 0. Conversely, if the signal
383 dominates the noise (i.e., SNR ≥ 1), the correction in equation (3) has a slight influence, and thus the
384 constrained future Earth system variable $\overline{y_c}$ with its variance can be estimated by equations (5) and
385 (6), respectively.

386 $$\overline{y_c} = \overline{y} + \frac{a}{1+SNR^{-1}}(\overline{x_0} - \overline{x}) \quad (5)$$

387 $$\sigma_{y_c}^2 = (1 - \frac{\rho^2}{1+SNR^{-1}})\sigma_y^2 \quad (6)$$

388

389 **References**

390 1. Anav, A., Murray-Tortarolo, G., Friedlingstein, P., Sitch, S., Piao, S., & Zhu, Z. (2013).
391 Evaluation of land surface models in reproducing satellite Derived leaf area index over the
392 high-latitude northern hemisphere. Part II: Earth system models. Remote. Sens. 5, 3637–3661.
393 https://doi.org/10.3390/rs5083637.

2. Parker, G. G. (2020). Tamm review: leaf area index (LAI) is both a determinant and a consequence of important processes in vegetation canopies. Forest. Ecol. Manag. 477, 118496. https://doi.org/10.1016/j.foreco.2020.118496.

3. Zhao, Q., Zhu, Z., Zeng, H., Zhao, W., & Myneni, R. B. (2020). Future greening of the Earth may not be as large as previously predicted. Agr. Forest. Meteorol. 292, 108111. https://doi.org/10.1016/j.agrformet.2020.108111.

4. Chen, J. M., Ju, W., Ciais, P., Viovy, N., Liu, R., Liu, Y., & Lu, X. (2019). Vegetation structural change since 1981 significantly enhanced the terrestrial carbon sink. Nat. Commun. 10, 4259. https://doi.org/10.1038/s41467-019-12257-8.

5. Burnham, J. H., & Sletten, R. S. (2010). Spatial distribution of soil organic carbon in Northwest Greenland and underestimates of high Arctic carbon stores. Global. Biogeochem. Cy. 24, GB3012. https://doi.org/10.1029/2009GB003660.

6. Launiainen, S., Katul, G. G., Kolari, P., Lindroth, A., Lohila, A., Aurela, M., Varlagin, A., Grelle, A., & Vesala, T. (2016). Do the energy fluxes and surface conductance of boreal coniferous forests in Europe scale with leaf area?. Global. Change. Biol. 22, 4096–4113. https://doi.org/10.1111/gcb.13497.

7. Miao, C., Immerzeel, W. W., Xu, B., Yang, K., Duan, Q., & Li, X. (2024). Understanding the Asian water tower requires a redesigned precipitation observation strategy. P. Natl. Acad. Sci. Usa. 121, e2403557121. https://doi.org/10.1073/pnas.2403557121.

8. Liu, Y., Kumar, M., Katul, G. G., Feng, X., & Konings, A. G. (2020). Plant hydraulics accentuates the effect of atmospheric moisture stress on transpiration. Nat. Clim. Change. 10, 691–695. https://doi.org/10.1038/s41558-020-0781-5.

9. Cheng, L., Zhang, L., Wang, Y. P., Canadell, J. G., Chiew, F. H., Beringer, J., Li, L., Miralles, D. G., Piao, S., Zhang, Y. (2017). Recent increases in terrestrial carbon uptake at little cost to the water cycle. Nat. Commun. 8, 110. https://doi.org/10.1038/s41467-017-00114-5.

10. Kumar, S. V., Mocko, D. M., Wang, S., Peters-Lidard, C. D., & Borak, J. (2019). Assimilation of remotely sensed leaf area index into the Noah-MP land surface model: Impacts on water and carbon fluxes and states over the continental United States. J. Hydrometeorol. 20, 1359–1377. https://doi.org/10.1175/JHM-D-18-0237.1.

11. Asaadi, A., Arora, V. K., Melton, J. R., & Bartlett, P. (2018). An improved parameterization of leaf area index (LAI) seasonality in the Canadian Land Surface Scheme (CLASS) and Canadian Terrestrial Ecosystem Model (CTEM) modelling framework. Biogeosciences. 15(22), 6885–6907. https://doi.org/10.5194/bg-15-6885-2018.

12. Kucharik, C. J., Barford, C. C., El Maayar, M., Wofsy, S. C., Monson, R. K., & Baldocchi, D. D. (2006). A multiyear evaluation of a Dynamic Global Vegetation Model at three AmeriFlux forest sites: Vegetation structure, phenology, soil temperature, and CO_2 and H_2O vapor exchange. Ecol. Model. 196, 1-31. https://doi.org/10.1016/j.ecolmodel.2005.11.031.

13. Anav, A., Friedlingstein, P., Kidston, M., Bopp, L., Ciais, P., Cox, P., Jones, C., Jung, M., Myneni, R., Zhu, Z. (2013). Evaluating the land and ocean components of the global carbon cycle in the CMIP5 earth system models. J. Climate. 26(18), 6801–6843. https://doi.org/10.1175/JCLI-D-12-00417.1.

14. Jiapaer, G., Liang, S., Yi, Q., & Liu, J. (2015). Vegetation dynamics and responses to recent climate change in Xinjiang using leaf area index as an indicator. Ecol. Indic. 58, 64–76. https://doi.org/10.1016/j.ecolind.2015.05.036.

15. Shang, X., He, Z., Chen, W., He, L., & Yang, H. (2023). Changes and response mechanisms of leaf area index and evapotranspiration in the typical natural landscapes of the Loess Plateau in northern Shaanxi of China under the human intervention. Ecol. Indic. 154, 110517. https://doi.org/10.1016/j.ecolind.2023.110517.

16. Chen, X., Cai, A., Guo, R., Liang, C., & Li, Y. (2023). Variation of gross primary productivity dominated by leaf area index in significantly greening area. J. Geogr. Sci. 33(8), 1747–1764. https://doi.org/10.1007/s11442-023-2151-5.

17. Li, Q., Lu, X., Wang, Y., Huang, X., Cox, P. M., & Luo, Y. (2018). Leaf area index identified as a major source of variability in modeled CO_2 fertilization. Biogeosciences. 15(22), 6909–6925. https://doi.org/10.5194/bg-15-6909-2018.

18. Zhao, W., Tan, W., & Li, S. (2021) High leaf area index inhibits net primary production in global temperate forest ecosystems. Environ. Sci. Pollut. R. 28(18), 22602–22611. https://doi.org/10.1007/s11356-020-11928-0.

19. Dong, N., Luo, M., Liu, Z., Sun, J., Wu, K., & Lin, H. (2021). The roles of leaf area index and albedo in vegetation induced temperature changes across China using modelling and observations. Clim. Dynam. 58, 2557–2573. https://doi.org/10.1007/s00382-021-06028-9.

20. Kala, J., Decker, M., Exbrayat, J. F., Pitman, A. J., Carouge, C., Evans, J. P., Abramowitz, G., Mocko, D. (2014). Influence of leaf area index prescriptions on simulations of heat, moisture, and carbon fluxes. J. Hydrometeorol. 15, 489–503. https://doi.org/10.1175/JHM-D-13-063.1.

21. Zhang, J., & Walsh, J. E. (2007). Relative impacts of vegetation coverage and leaf area index on climate change in a greener north. Geophys. Res. Lett. 34(15), L15703. https://doi.org/10.1029/2007GL030852.

22. Tokarska, K. B., Stolpe, M. B., Sippel, S., Fischer, E. M., Smith, C. J., Lehner, F., & Knutti, R. (2020). Past warming trend constrains future warming in CMIP6 models. Sci. Adv. 6, eaaz9549. https://doi.org/10.1126/sciadv.aaz9549.

23. Chai, Y., Martins, G., Nobre, C., von Randow, C., Chen, T., & Dolman, H. (2021). Constraining Amazonian land surface temperature sensitivity to precipitation and the probability of forest dieback. Npj. Clim. Atmos. Sci. 4, 6. https://doi.org/10.1038/s41612-021-00162-1.

24. Chai, Y., Berghuijs, W. R., Naudts, K., Janssen, T. A., Yao, Y., & Dolman, H. (2021). Using precipitation sensitivity to temperature to adjust projected global runoff. Environ. Res. Lett. 16, 124032. https://doi.org/10.1088/1748-9326/ac3795.

25. Hall, A., & Qu, X. (2006). Using the current seasonal cycle to constrain snow albedo feedback in future climate change. Geophys. Res. Lett. 33, L03502. https://doi.org/10.1029/2005GL025127.

26. Cox, P. M., Huntingford, C., & Williamson, M. S. (2018). Emergent constraint on equilibrium climate sensitivity from global temperature variability. Nature. 553, 319–322. https://doi.org/10.1038/nature25450.

27. Cox, P. M., Pearson, D., Booth, B. B., Friedlingstein, P., Huntingford, C., Jones, C. D., & Luke, C. M. (2013). Sensitivity of tropical carbon to climate change constrained by carbon dioxide variability. Nature, 494(7437), 341–344. https://doi.org/10.1038/nature11882.

28. Wenzel, S., Cox, P. M., Eyring, V., & Friedlingstein, P. (2016). Projected land photosynthesis constrained by changes in the seasonal cycle of atmospheric CO_2. Nature. 538, 499–501. https://doi.org/10.1038/nature19772.

29. Sitch, S., Friedlingstein, P., Gruber, N., Jones, S. D., Murray-Tortarolo, G., Ahlström, A., Doney, S. C., Graven, H., Heinze, C., Huntingford, C. et al. (2015). Recent trends and drivers of

regional sources and sinks of carbon dioxide. Biogeosciences. 12(3), 653–679. https://doi.org/10.5194/bg-12-653-2015.

30. Liu, Y., Liu, R., & Chen, J. M. (2012). Retrospective retrieval of long-term consistent global leaf area index (1981–2011) from combined AVHRR and MODIS data. J. Geophys. Res-Biogeo. 117(G4), G04003. https://doi.org/10.1029/2012JG002084.
31. Xiao, Z., Liang, S., Wang, J., Chen, P., Yin, X., Zhang, L., & Song, J. (2013). Use of general regression neural networks for generating the GLASS leaf area index product from time-series MODIS surface reflectance. IEEE. T. Geosci. Remote. 52, 209–223. https://doi.org/10.1109/TGRS.2013.2237780.
32. Cao, S., Li, M., Zhu, Z., Wang, Z., Zha, J., Zhao, W., Duanmu, Z., Chen, J., Zheng, Y., Chen, Y. et al. (2023). Spatiotemporally consistent global dataset of the GIMMS leaf area index (GIMMS LAI4g) from 1982 to 2020. Earth. Syst. Sci. Data. 15, 4877–4899. https://doi.org/10.5194/essd-15-4877-2023.
33. Bowman, K. W., Cressie, N., Qu, X., & Hall, A. (2018). A hierarchical statistical framework for emergent constraints: Application to snow-albedo feedback. Geophys. Res. Lett. 45(23), 13050–13059. https://doi.org/10.1029/2018GL080082.
34. Winkler, A. J., Myneni, R. B., & Brovkin, V. (2019). Investigating the applicability of emergent constraints. Earth. Syst. Dynam. 10(3), 501–523. https://doi.org/10.5194/esd-10-501-2019.
35. Hall, A., Cox, P., Huntingford, C., & Klein, S. (2019). Progressing emergent constraints on future climate change. Nat. Clim. Change. 9, 269–278. https://doi.org/10.1038/s41558-019-0436-6.

503 36. Williamson, M. S., Thackeray, C. W., Cox, P. M., Hall, A., Huntingford, C., & Nijsse, F. J.
504 (2021). Emergent constraints on climate sensitivities. Rev. Mod. Phys. 93(2), 025004.
505 https://doi.org/10.1103/RevModPhys.93.025004.
506 37. Hatfield, J. L., & Dold, C. (2019). Photosynthesis in the solar corridor system. In The solar
507 corridor crop system (pp. 1-33). Academic Press.
508 https://doi.org/10.1016/B978-0-12-814792-4.00001-2.
509 38. Yan, Y., Hou, P., Duan, F., Niu, L., Dai, T., Wang, K., Zhao, M., Li, S., & Zhou, W. (2021).
510 Improving photosynthesis to increase grain yield potential: an analysis of maize hybrids released
511 in different years in China. Photosynth. Res. 150, 295–311.
512 https://doi.org/10.1007/s11120-021-00847-x.
513 39. van Loon, M. P., Schieving, F., Rietkerk, M., Dekker, S. C., Sterck, F., & Anten, N. P. (2014).
514 How light competition between plants affects their response to climate change. New Phytol.
515 203(4), 1253–1265. https://doi.org/10.1111/nph.12865.
516 40. Hoff, C., & Rambal, S. (2003). An examination of the interaction between climate, soil and leaf
517 area index in a Quercus ilex ecosystem. Ann. Forest. Sci. 60(2), 153–161.
518 https://doi.org/10.1051/forest:2003008.
519 41. Seo, H., & Kim, Y. (2021). Role of remotely sensed leaf area index assimilation in
520 eco-hydrologic processes in different ecosystems over East Asia with Community Land Model
521 version 4.5–Biogeochemistry. J. Hydrol. 594, 125957.
522 https://doi.org/10.1016/j.jhydrol.2021.125957.
523 42. Wen, N., Han, Y., Qi, J., Marek, G. W., Sun, D., Feng, P., Srinivasan, R., Liu, D., & Chen, Y.
524 (2024). Improving hydrological modeling to close the gap between elevated CO_2 concentration

525 and crop response: Implications for water resources. Water. Res. 265, 122279.
526 https://doi.org/10.1016/j.watres.2024.122279.
527 43. Peters, E. B., & McFadden, J. P. (2010). Influence of seasonality and vegetation type on
528 suburban microclimates. Urban. Ecosyst. 13, 443–460.
529 https://doi.org/10.1007/s11252-010-0128-5.
530 44. Baker, T. P., Jordan, G. J., Steel, E. A., Fountain-Jones, N. M., Wardlaw, T. J., & Baker, S. C.
531 (2014). Microclimate through space and time: microclimatic variation at the edge of
532 regeneration forests over daily, yearly and decadal time scales. Forest. Ecol. Manag. 334, 174–
533 184. https://doi.org/10.1016/j.foreco.2014.09.008.
534 45. Sándor, R., & Fodor, N. (2012). Simulation of soil temperature dynamics with models using
535 different concepts. Sci. World. J. 2012, 590287. https://doi.org/10.1100/2012/590287.
536 46. Lian, X., Piao, S., Huntingford, C., Li, Y., Zeng, Z., Wang, X., Ciais, P., McVicar, T. R., Peng, S.,
537 Ottlé, C. et al. (2018). Partitioning global land evapotranspiration using CMIP5 models
538 constrained by observations. Nat. Clim. Change. 8, 640–646.
539 https://doi.org/10.1038/s41558-018-0207-9.
540 47. Alkama, R., Forzieri, G., Duveiller, G., Grassi, G., Liang, S., & Cescatti, A. (2022).
541 Vegetation-based climate mitigation in a warmer and greener World. Nat. Commun. 13, 606.
542 https://doi.org/10.1038/s41467-022-28305-9.
543 48. Skinner, C. B., Poulsen, C. J., & Mankin, J. S. (2018). Amplification of heat extremes by plant
544 CO_2 physiological forcing. Nat. Commun. 9, 1094.
545 https://doi.org/10.1038/s41467-018-03472-w.

546 49. Piao, S., Wang, X., Park, T., Chen, C., Lian, X. U., He, Y., Bjerke, J. W., Chen, A., Ciais, P.,
547 Tømmervik, H. et al. (2020). Characteristics, drivers and feedbacks of global greening. Nat. Rev.
548 Earth. Env. 1, 14–27. https://doi.org/10.1038/s43017-019-0001-x.
549 50. Zhu, Z., Piao, S., Myneni, R. B., Huang, M., Zeng, Z., Canadell, J. G., Ciais, P., Sitch, S.,
550 Friedlingstein, P., Arneth, A. (2016). Greening of the Earth and its drivers. Nat. Clim. Change. 6,
551 791–795. https://doi.org/10.1038/nclimate3004.
552 51. Wang, S., Zhang, Y., Ju, W., Chen, J. M., Ciais, P., Cescatti, A., Sardans, j., Janssens, I. A., Wu,
553 M., Berry, J. A. et al. (2020). Recent global decline of CO_2 fertilization effects on vegetation
554 photosynthesis. Science. 370, 1295–1300. https://doi.org/10.1126/science.abb7772.
555 52. Piao, S., Sitch, S., Ciais, P., Friedlingstein, P., Peylin, P., Wang, X., Ahlström, A., Anav, A.,
556 Canadell, J. G., Cong, N. et al. (2013). Evaluation of terrestrial carbon cycle models for their
557 response to climate variability and to CO_2 trends. Global. Change. Biol. 19, 2117–2132.
558 https://doi.org/10.1111/gcb.12187.
559 53. Jones, C. D., Arora, V., Friedlingstein, P., Bopp, L., Brovkin, V., Dunne, J., Graven, H., Hoffman,
560 F., Ilyina, T., John, J. G. et al. (2016). C4MIP–The coupled climate–carbon cycle model
561 intercomparison project: Experimental protocol for CMIP6. Geosci. Model. Dev. 9, 2853–2880.
562 https://doi.org/10.5194/gmd-9-2853-2016.
563 54. Cook, B. I., Mankin, J. S., Marvel, K., Williams, A. P., Smerdon, J. E., & Anchukaitis, K. J.
564 (2020). Twenty-first century drought projections in the CMIP6 forcing scenarios. Earths. Future.
565 8, e2019EF001461. https://doi.org/10.1029/2019EF001461.
566 55. Duveiller, G., Hooker, J. & Cescatti, A. (2018). The mark of vegetation change on Earth's
567 surface energy balance. Nat. Commun. 9, 679. https://doi.org/10.1038/s41467-017-02810-8.

568 56. Hoek van Dijke, A. J., Mallick, K., Schlerf, M., Machwitz, M., Herold, M., & Teuling, A. J.
569 (2020). Examining the link between vegetation leaf area and land–atmosphere exchange of water,
570 energy, and carbon fluxes using FLUXNET data. Biogeosciences, 17, 4443–4457.
571 https://doi.org/10.5194/bg-17-4443-2020.

572 57. Zeng, Z., Piao, S., Li, L. Z., Zhou, L., Ciais, P., Wang, T., Li, Y., Lian, X., Wood, E. F.,
573 Friedlingstein, P. et al. (2017). Climate mitigation from vegetation biophysical feedbacks during
574 the past three decades. Nat. Clim. Change. 7, 432–436. https://doi.org/10.1038/nclimate3299.

575 58. He, M., Piao, S., Huntingford, C., Xu, H., Wang, X., Bastos, A., Cui, J., Gasser, T. (2022).
576 Amplified warming from physiological responses to carbon dioxide reduces the potential of
577 vegetation for climate change mitigation. Commun. Earth. Environ. 3, 160.
578 https://doi.org/10.1038/s43247-022-00489-4.

579 59. Park, H., & Jeong, S. (2021). Leaf area index in Earth system models: how the key variable of
580 vegetation seasonality works in climate projections. Environ. Res. Lett. 16, 034027.
581 https://doi.org/10.1088/1748-9326/abe2cf.

582 60. Xiao, Z., Wang, T., Liang, S., & Sun, R. (2016). Estimating the fractional vegetation cover from
583 GLASS leaf area index product. Remote. Sens. 8(4), 337. https://doi.org/10.3390/rs8040337.

584 61. Fang, H., Jiang, C., Li, W., Wei, S., Baret, F., Chen, J. M., Garcia-Haro, J., Liang, S., Liu, R.,
585 Myneni, R. B. et al. (2013). Characterization and intercomparison of global moderate resolution
586 leaf area index (LAI) products: Analysis of climatologies and theoretical uncertainties. J.
587 Geophys. Res-Biogeo. 118, 529–548. https://doi.org/10.1002/jgrg.20051.

588 62. Wikle, C. K., & Berliner, L. M. (2007). A Bayesian tutorial for data assimilation. Physica. D.
589 230, 1–16. https://doi.org/10.1016/j.physd.2006.09.017.

63. Kang, E. L., & Cressie, N. (2013). Bayesian hierarchical ANOVA of regional climate-change projections from NARCCAP Phase II. Int. J. Appl. Earth. Obs. 22, 3–15. https://doi.org/10.1016/j.jag.2011.12.007.

64. Katzfuss, M., Hammerling, D., & Smith, R. L. (2017). A Bayesian hierarchical model for climate change detection and attribution. Geophys. Res. Lett. 44(11), 5720–5728. https://doi.org/10.1002/2017GL073688.

65. Chen, X., Zhou, T., Wu, P., Guo, Z., & Wang, M. (2020). Emergent constraints on future projections of the western North Pacific Subtropical High. Nat. Commun. 11, 2802. https://doi.org/10.1038/s41467-020-16631-9.

Resource Availability

Lead contact:

Further information and requests for resources and reagents should be directed to and will be fulfilled by the lead contact, Chiyuan Miao (miaocy@bnu.edu.cn).

Materials availability: *This research generated no novel materials*

Data and Code availability

The observed LAI was obtained from three datasets: GLASS LAI (http://www.geodata.cn/data/index.html?word=GLASS), GLOBMAP LAI (https://zenodo.org/record/4700264#.Ye5xwStzy70) and GIMMS LAI4g (https://zenodo.org/records/8035760). The observed air temperature and precipitation were provided by the HadCRUT4 dataset (http://www.cru.uea.ac.uk/). Simulations from the CMIP6 models were collected from https://esgf-node.llnl.gov/projects/cmip6/. Some models lack the r1i1p1f1 output but

provide the r1i1p1f2 output instead. Due to the high consistency in LAI values between these two outputs, we adopt r1i1p1f2 as a replacement for models missing r1i1p1f1. The atmospheric CO_2 concentration data were obtained from https://tntcat.iiasa.ac.at/SspDb/dsd?Action=htmlpage&page=about. Simulations from the CMIP5 models were corrected from https://esgf-node.llnl.gov/projects/cmip5/. The TRENDY-v9 model simulations under the three controlled experiments of S1, S2 and S3 can be obtained by contacting Stephen Sitch (s.a.sitch@exeter.ac.uk) and Pierre Friedlingstein (p.friedlingstein@exeter.ac.uk). The code for this study is available at https://github.com/Yuanchai1/Climate-projections-underestimate-future-global-land-greening-and-terrestrial-water-losses.git.

Acknowledgements

We are thankful to Prof. Peter Cox and Prof. Han Dolman for their helpful comments and valuable suggestions for this paper. Y.C. acknowledges support from the National Natural Science Foundation of China (42301018). C.M. acknowledges support from the National Natural Science Foundation of China (U24A20572) and the National Key Research and Development Program of China (2024YFF0809301). L.S. acknowledges support from UKRI (MR/V022008/1).

Author contributions

Conceptualization, Y.C. and C.M.; methodology, Y.C. and C.M.; investigation, Y.C. and C.M.; writing—original draft, Y.C. and C.M.; writing—review & editing, P.C., L.S., W. R. B., T.C. and C.H.; funding acquisition, C.M.; resources, Y.C. and C.M.; supervision, C.M.

Competing interests

The authors declare no competing interests.

Additional information

Correspondence and requests for materials should be addressed to C.M.

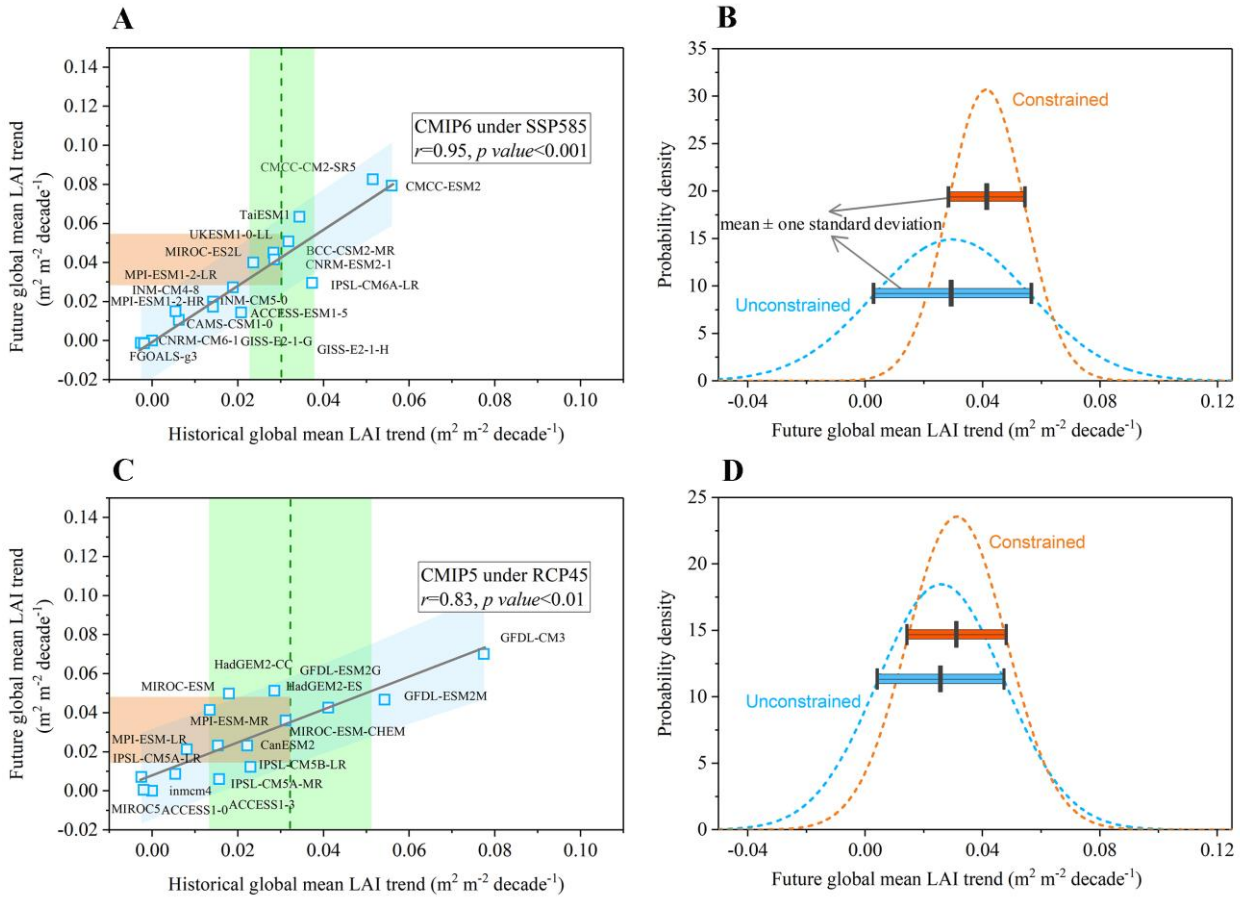

Figure 1. Emergent constraints on future global mean LAI trends. **A** and **C**, The emergent relationships between the historical and future global mean LAI trends in the CMIP6 model ensemble (1982–2014 and 2015–2100 under scenario SSP585) and in the CMIP5 ensemble (1982–2005 and 2015–2100 under RCP45), respectively. The vertical green shadings in **A** and **C** are the observed estimates of global LAI trends (mean ± one standard deviation) based on the three observational datasets. The horizontal orange shading indicates the new constrained estimates of future global LAI trends (mean ± one standard deviation) after application of the emergent constraint. The light blue shadings are the error of the regression lines. **B** and **D**, The probability density functions (PDFs) of the original ESM global greening trend projections (dashed light-blue line), and of the updated global greening trend projections obtained by applying the observational constraint (dashed orange line) to the CMIP6 and CMIP5 model ensembles, respectively. The horizontal boxplots show the future global LAI trends (mean ± one standard deviation).

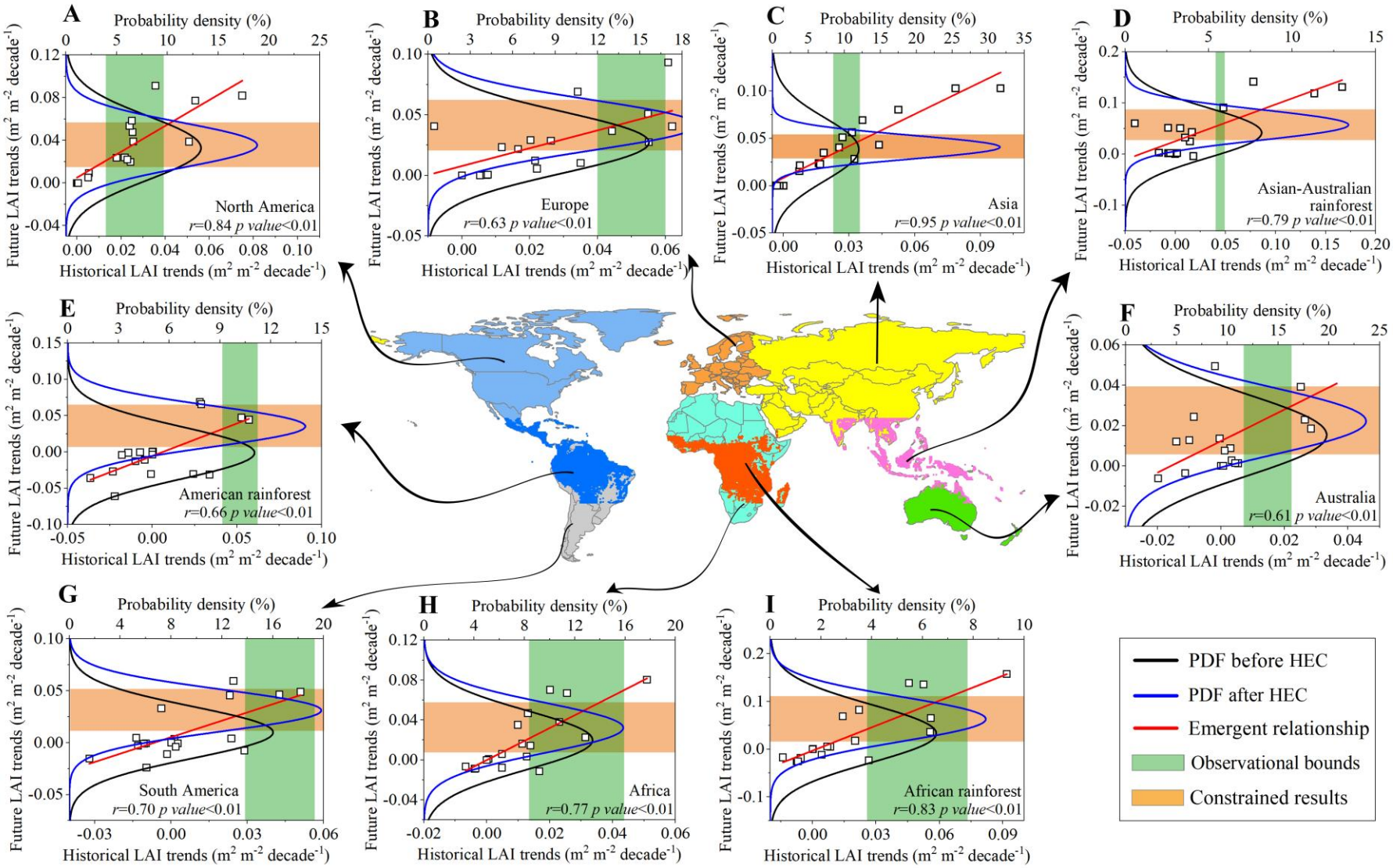

Figure 2. Emergent constraints on the future LAI trends in nine sub-regions of the global land surface for the CMIP6 models under the SSP585 emission scenario. Presented are the emergent relationships between historical LAI trends (1982–2014, m^2 m^{-2} $decade^{-1}$) and future LAI trends (2015–2100, m^2 m^{-2} $decade^{-1}$) in the nine sub-regions of North America (**A**), Europe (**B**), Asia (**C**), the Asian-Australian rainforest

(**D**), the American rainforest (**E**), Australia (**F**), South America (**G**), Africa (**H**) and the African rainforest (**I**). The term "rainforest" is used to refer to tropical regions with rainforest (rainforest regions overlap with the continent regions). Black and blue curves are the PDFs of the future LAI trends before and after using the hierarchical emergent constraint procedure (HEC), respectively. Vertical green shadings are the observed estimates of LAI trends (mean ± one standard deviation) based on the three datasets. Horizontal orange shadings are the constrained future LAI trend (mean ± one standard deviation). Square markers are individual CMIP6 models. The central panel presents the geographical distributions of the nine sub-regions.

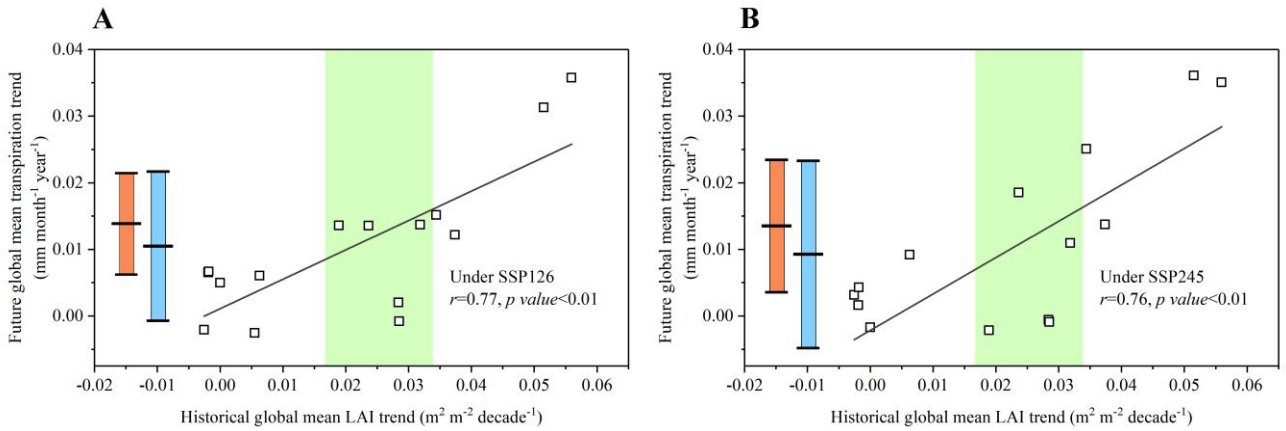

666

667 **Figure 3. Implications of underestimated global land greening trends for future global mean**
668 **transpiration trends under the low and middle emission pathways associated with the SSP126**
669 **and SSP245 scenarios.** The fitted line illustrates the emergent relationship between the historical
670 trends in global mean LAI (1982–2014) and the future projected trends in global mean transpiration
671 (2015–2100) across the CMIP6 models. **A** and **B**, The relationships under the SSP126 and SSP245
672 emission scenarios, respectively. Each square represents a CMIP6 model. Vertical green shadings are
673 the observed global mean LAI trends (mean ± one standard deviation). Box plots in each panel
674 indicate the mean value ± one standard error of the original model predictions of future transpiration
675 trends (light-blue box plots) and of the constrained future transpiration trend (orange box plots).